2024 IEEE/ASME International Conference on Advanced Intelligent Mechatronics (AIM)
July 15-19, 2024. Boston, MA, USA

Towards Ultrasonic Scalpel for Single-Port Robotic Surgery: Design of a Miniature Langevin Ultrasonic Transducer

Yuzhen Cao, Yue Ding, Chuanxiang Zhu, Haomin Kuang, Ren Zhao, and Kai Xu, *Member, IEEE*

***Abstract*— The manipulation difficulties in laparoscopic procedures inspire the development of surgical robotic systems. To perform tissue dissection and coagulation, electrosurgical instruments and ultrasonic scalpels are integrated. Ultrasonic scalpels, which utilize high-frequency vibration generated by ultrasonic transducer to dissect and coagulate tissues, are safer than electrosurgical instruments due to concentrated energy release. However, the rigid straight waveguides involved in conventional ultrasonic scalpels prevent their integration into single-port surgical robots, within which multi-joint articulated or continuum bendable instruments are used. Putting miniature transducers at the distal end of the instruments is a potential way to integrate ultrasonic scalpels. However, the existing miniature ultrasonic transducers arranged at instrument distal ends have limited energy efficiency due to their 55.5-kHz half-wavelength design. This paper hence proposes the design of a 6-mm 120-kHz full-wavelength miniature ultrasonic transducer. The proposed 120-kHz full-wavelength structure can provide sufficient energy efficiency while maintaining the transducer's compact size. Finite-element model is utilized to optimize the proposed transducer's structure. The tissue dissection capability of the proposed 120-kHz miniature ultrasonic scalpel is demonstrated experimentally. It's promising for the proposed design to be integrated into an 8 mm continuum instrument for single-port robotic surgery.**

I. Introduction

Laparoscopic surgery has become a widely adopted technique due to its advantages, such as lower postoperative complication rates, less pain, shorter recovery time, and better cosmesis [1]. Single-port laparoscopic surgery, which uses only one skin incision, demonstrated better surgical outcomes [2]. However, the manipulation difficulties in laparoscopic procedures inspire the development of surgical robot systems [3-5].

To perform efficient tissue dissection and coagulation, electrosurgical instruments and ultrasonic scalpels are used. Ultrasonic scalpels utilize high-frequency mechanic vibration generated by a piezoelectric-based ultrasonic transducer to perform operation, and are considered safer since they are smokeless, bring less thermal damage, and take no current through tissue [6]. On the other hand, safety issues related to electrosurgical instruments are reported [7].

Conventional ultrasonic scalpel involves a rigid straight waveguide to transfer ultrasonic vibrations from the proximal ultrasonic transducer to the distal tip, as shown in Fig. 1 (a). This structure prevents its integration into the single-port surgical robot, within which multi-joint articulated or continuum bendable instruments are used.

To expand the applicability of ultrasonic scalpels, one way is to use bendable waveguides. Wakako *et al.* [8] developed a bendable ultrasonic scalpel by utilizing a pre-curved super elasticity alloy rod as a waveguide. However, the vibration amplitude is insufficient after bending. The other potential way is to put a miniature piezoelectric-based ultrasonic transducer at the distal end of the instruments to integrate ultrasonic scalpels. Khalaji *et al.* [9] developed a 55.5-kHz miniature ultrasonic transducer with an 8 mm outer diameter for its integration with a da Vinci surgical instrument. Li *et al.* [10] designed a 55.5-kHz ultrasonic transducer with a 10 mm diameter and connected it with a rigid shaft through a snake-like joint. Although these miniature transducers with 8- or 10-mm diameters have been proposed to fulfill the minimum requirement of tissue dissection and coagulation, the radial dimension limits the volume of the piezo stack, resulting in insufficient output power and poor operation efficiency if the 55.5-kHz half-wavelength structure is adopted [11].

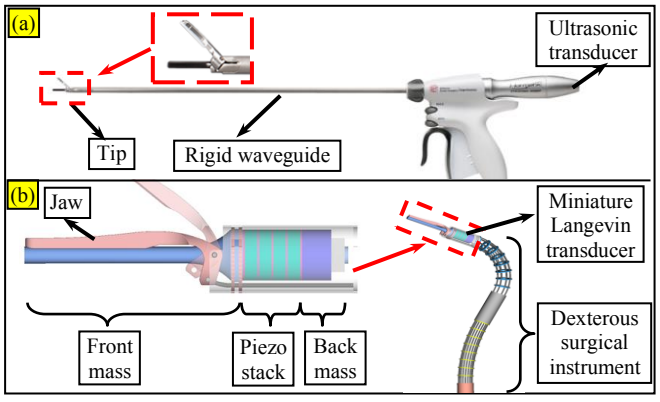

Fig. 1 Ultrasonic surgical scalpel: (a) a conventional hand-held ultrasonic scalpel, (b) the proposed ultrasonic scalpel for single-port robotic surgery.

The total length of an ultrasonic transducer is the wavelength of its vibration standing wave. At the resonance frequency (55.5kHz) of commercial ultrasound surgical scalpels, designs of the miniature ultrasound transducers are limited to half-wavelength structures to meet length requirements for laparoscopic surgeries. This design features a single node, necessitating its placement outside the piezo

*Research supported in part by the National Key R&D Program of China (Grant No. 2022YFB4700900, Grant No. 2019YFC0118003, and Grant No. 2019YFC0118004), and in part by the National Natural Science Foundation of China (Grant No. 51722507).

Yuzhen Cao, Yue Ding, Chuanxiang Zhu, Haomin Kuang ,and Kai Xu are with the State Key Laboratory of Mechanical System and Vibration, School of Mechanical Engineering, Shanghai Jiao Tong University, Shanghai, 200240, China (e-mails: Cymber-Z@sjtu.edu.cn, dingyue2020@sjtu.edu.cn, zcx_sjtu@sjtu.edu.cn, kuang_hm@sjtu.edu.cn, and k.xu@sjtu.edu.cn; corresponding author: Kai Xu)

Ren Zhao is with Department of General Surgery, Shanghai Institute of Digestive Surgery, Ruijin Hospital, Shanghai Jiao Tong University School of Medicine, Shanghai, China (zhaorensurgeon@aliyun.com).

stack for transducer installation. Consequently, this 55.5 kHz half-wavelength design leads to an increase in structural damping [12], resulting in poor energy conversion efficiency.

Towards an ultrasonic scalpel with improved efficiency for single-port robotic surgery, this work proposes a full-wavelength ultrasonic transducer with an outer diameter of only 6 mm, where one of the two nodes is positioned inside the piezo stack. By increasing the transducer's resonant frequency to 120 kHz, it is potential to enhance the output power while maintaining a miniature total length for dexterous movements in surgery, potentially achieving higher operation efficiency over the existing miniature ultrasonic transducers.

The rest of this paper is organized as follows. Section II explains the design of the full-wavelength miniature transducer. The vibration model and the finite-element structural optimization of the transducer are elaborated. Experimental validations are presented in Section III. The conclusion and future works are summarized in Section IV.

II. Design, Vibration Model, and Structural Optimization of the Ultrasonic Transducer

The structural design of the 120-kHz full-wavelength miniature ultrasonic transducer is summarized in Section II.A. The vibration model of the transducer is first used to determine the transducer's structural parameters as presented in Section II.B. The finite-element model and structural parameters optimization of the transducer are elaborated in Section II.C.

A. Design of the Ultrasonic Transducer

Langevin-type transducers are widely applied in power ultrasonic systems. As shown in Fig. 1 (b), a Langevin ultrasonic transducer consists of a front mass, a back mass, and a piezo stack compressed between them. When applying a high-frequency voltage to the piezo stack, mechanical vibration of the same frequency will be generated.

The structural details of the full-wavelength miniature transducer are shown in Fig. 2(a). The structure of a half-wavelength transducer is also presented for comparison in Fig. 2(b).

For the full-wavelength transducers, one of the vibration nodes is designed within the front mass, where the mounting flange is located. A cutting tip (a rod structure with a relatively small cross-section) intended for tissue interaction is designed at the end of the front mass. To reduce stress concentration, a transition structure is used for the smooth transition of the front mass's larger cross-section and the cutting tip. A stack of 4 piezo rings placed between the front mass and the back mass is used to generate ultrasonic vibration. Copper electrodes are placed at the interfaces of the piezo rings. A nut is used to pre-compress the piezo stack, by fitting with the screw located at the front mass.

To facilitate dexterous instrument movements in laparoscopic intervention, the transducer's total length should be as short as possible, ideally not exceeding 40 mm. The outer diameter of the full-wavelength transducer is set to 6 mm since it is aimed to be fitted into the 8 mm outer diameter continuum surgical instrument when incorporated into the single-port surgical robot [5]. The cutting tip of the front mass is set to have a diameter of 2 mm, according to existing ultrasonic scalpels. An M2 nut is used to compress the piezo stack. Hence the piezo ring with the electrodes has an inner diameter of 2.4 mm, leaving room for an isolating tube. The M2 compressing nut has a standard length L_1 of 1.6 mm. The thickness of the piezo ring and the electrode are 1.5 mm and 0.2 mm, respectively, according to the supplier's stock specification. The undetermined structural parameters L_2, L_4, L_5, and L_6 are to be calculated by the transducer's vibration model.

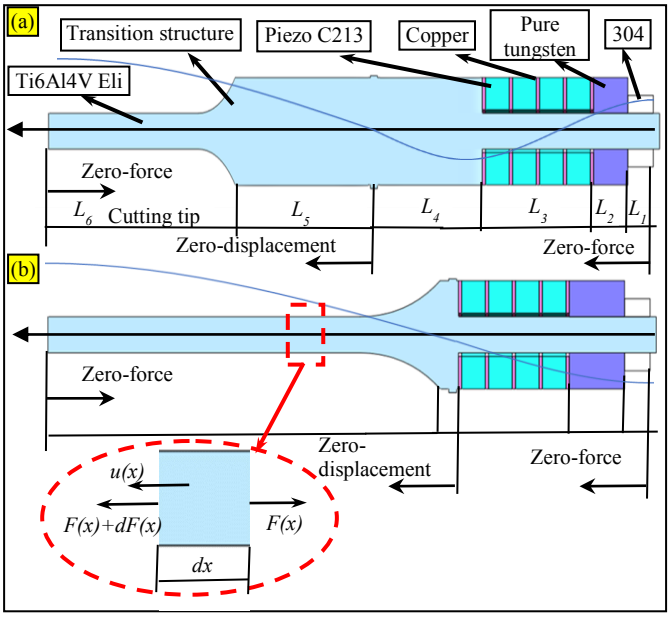

Fig. 2 Structure and materials of the miniature ultrasonic transducer: (a) the full-wavelength transducer, (b) the half-wavelength transducer.

The material of each component is shown in Fig. 2, while the material parameters are shown in Table I and Table II. The front mass's material is chosen as the Ti6Al4V-Eli due to its biocompatibility and acoustic properties. Pure tungsten is selected as the material of the back mass since it has a high acoustic impedance, which contributes to the transducer's miniaturization. The Fuji C-213 ceramics (Fuji Ceramics Corporation) is chosen as the piezo material due to its high mechanical quality factor. The density, relative dielectric constant $\boldsymbol{\varepsilon}$, flexibility matrix $\mathbf{s}^{\mathbf{E}}$, and coupling matrix $\mathbf{d}$ are referred to the Fuji Ceramics Corporation datasheet.

TABLE I. Parameters of Non-Piezo Materials

Material	Young's modulus (Pa)	Poisson rate	Density/(kg/m^3)
Ti6Al4V-Eli	1.1×10^{11}	0.32	4470
Pure tungsten	3.4×10^{11}	0.2	19270
304	2.6×10^{11}	0.28	7930

TABLE II. Parameters of C-213 Materials

ε_{11}	ε_{33}	Density/(kg/m^3)
1590	1470	7800
Y_{11} (N/m^2)	Y_{33} (N/m^2)	Y_{55} (N/m^2)
8.2×10^{10}	6.6×10^{10}	2.6×10^{10}
d_{31} (C/N)	d_{33} (C/N)	d_{15} (C/N)
-135×10^{-12}	310×10^{-12}	510×10^{-12}

B. Vibration Model of the Transducer

The vibration of the transducer can be modeled as the longitudinal vibration of a rod with a variable cross-section. The nomenclature used in this paper is shown in Table III.

TABLE III. NOMENCLATURE USED IN THIS PAPER

Symbol	Definition
i	Index of the transducer's structural segment, i = 1~6.
L_i	The longitudinal length of the transducer's i^{th} segment.
ρ_i	The density of the i^{th} segment's material.
E_i	The Young's modulus of the i^{th} segment's material.
t	Time.
x	Longitudinal coordinate along the transducer's axis.
x_i	The coordinate of the i^{th} and $(i+1)^{th}$ segments' interface.
$F(x)$	The internal force of the cross-section at coordinate x.
$u(x)$	The displacement of the cross-section at coordinate x.
$v(x)$	The vibration speed of the cross-section at coordinate x.
$S(x)$	The area of the cross-section at coordinate x.
f	The frequency of the vibration.
ω	The angle frequency of the vibration. $\omega=2\pi f$

As shown in Fig. 2 (b), the vibration equation of an arbitrary longitudinal element of the transducer can be formulated as Eq. (1).

$$(F(x)+dF(x))-F(x)=\rho_i S(x)dx\frac{\partial^2 u(x)}{\partial t^2} \tag{1}$$

$F(x)$ can be calculated by stress-strain representation in Eq. (2).

$$F(x)=E_i S(x)\frac{\partial u(x)}{\partial x} \tag{2}$$

By solving the vibration equation, the i^{th} segment's $|u(x)|$ can be derived as Eq. (3).

$$|u(x)|=\frac{1}{\sqrt{S(x)}}(A_i\sin K_i x+B_i\cos K_i x) \tag{3}$$

Where K_i is written in Eq. (4). A_i and B_i are constants that can be solved by the boundary conditions of each segment.

$$K_i^2=k_i^2-\frac{1}{\sqrt{S(x)}}\frac{\partial^2(\sqrt{S(x)})}{\partial x^2} \tag{4}$$

For the full-wavelength transducer, the zero-force boundary condition is applied to the two end faces of the transducer, while the zero-displacement boundary condition is applied to the interface of the 4th and 5th segments, where the mounting flange is placed, as shown in Fig. 2(a). The displacement and force continuity boundary conditions are applied to all the interfaces between adjacent segments. The frequency equations, Eq. (5) and Eq. (6) can be derived by solving Eq. (3) and the boundary conditions.

$$\frac{Z_6}{Z_5}\tan K_5L_5\tan K_6L_6=1 \tag{5}$$

Where $Z_i=E_iS(x_i^-)K_i$.

$$\begin{aligned}&\frac{Z_1}{Z_3}\tan k_1L_1\tan k_3L_3+\frac{Z_2}{Z_3}\tan k_2L_2\tan k_3L_3\\&+\frac{Z_1}{Z_2}\tan k_1L_1\tan k_2L_2+\frac{Z_1}{Z_4}\tan k_1L_1\tan k_4L_4\\&+\frac{Z_2}{Z_4}\tan k_2L_2\tan k_4L_4+\frac{Z_3}{Z_4}\tan k_3L_3\tan k_4L_4\\&=1+\frac{Z_1Z_3}{Z_2Z_4}\tan k_1L_1\tan k_2L_2\tan k_3L_3\tan k_4L_4\end{aligned} \tag{6}$$

With a given frequency f, Eq. (5) and Eq. (6) can be used to determine the length of the full-wavelength transducer's segments.

To meet the total length limitation of 40 mm, the vibration frequency of the full-wavelength transducer is increased to 120kHz. Utilizing Eq. (5) and Eq. (6), L_2 and L_4 are coupled, while L_5 and L_6 are coupled as well. Their values will be determined by the structural parameter optimization as presented in the next subsection.

C. Finite-element Model-Based Structural Optimization

A finite-element model of the transducer is used to optimize the structural parameters L_2, L_4, L_5, and L_6.

COMSOL Multiphysics 5.6 (Burington, MA) is utilized to perform the FEM (finite-element method) analysis. The solid mechanic module and the static electricity module are used to calculate the displacement and electric fields, respectively. The two modules are coupled by the piezoelectric equations as in Eq. (7).

$$\begin{cases}\mathbf{S}=\mathbf{s}^{\mathbf{E}}\mathbf{T}+\mathbf{d}^T\mathbf{E}\\ \mathbf{D}=\mathbf{dT}+\boldsymbol{\varepsilon}\mathbf{E}\end{cases} \tag{7}$$

Where **S** and **T** are the strain and stress respectively. **D** and **E** are the electric displacement and electric field. $\mathbf{s}^{\mathbf{E}}$ and **d** are the flexibility matrix and coupling matrix.

According to the formula for the ultrasound transducer damping [12], Rayleigh damping is employed in harmonic response analysis with damping coefficients set as $\alpha = 0$ and $\beta = 1/(\omega \cdot Q_m)$, where ω is the resonant angular frequency of the transducer, and Q_m is the mechanical quality factor. According to existing research, the Q_m value is usually between 600 and 700. An approximate value of 650 is used here for the optimization.

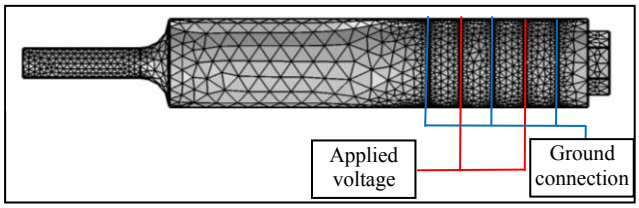

Fig. 3 Mesh and boundary conditions of the finite-element analysis.

The boundary conditions are shown in Fig. 3. In the solid mechanic module, the free boundary condition is applied to the surfaces. In the static electric module, the zero electric potential boundaries are applied to the selected end surfaces of the piezo rings, while the constant electric potential boundary condition is applied to the opposite end surfaces.

The mesh generator of COMSOL is used to generate the finite-element mesh.

The transition structure of the front mass is a design variable that affects the overall length, amplitude, and stress distribution of the transducer. This study first investigated the effects of various transition section structures and lengths on stress distribution and vibration speed voltage ratio, including step-shape, catenary, conical, and rounding-corner transition structures of different dimensions. Comparing the performance of different transition section structures under the parameter values of L_2 = 2.0 mm and L_6 = 10.0 mm. At the 120-kHz vibration frequency and 9.2μm amplitude, the corresponding finite-element simulation results are shown in Fig. 4. Design parameters and corresponding performance indicators are summarized in Table IV (rows correspond to Fig. 4 (a)-(h) in order): i) the step-shape transducer can achieve the shortest total length and most compact design. However, due to the sudden changes in shape, the stress concentration of the step-shape transducer is the highest; ii) compared to other structures, the catenary-shape transducer has lower maximum s4tress, but increasing the transition length results in a significant decrease in output vibration speed per unit voltage. Additionally, the catenary and the conical transducers have excessive total lengths, exceeding the specified requirements; iii) the transducer with a 2-mm radius rounding corner has the maximum vibration speed voltage ratio.

Based on the above analyses, the transducer with a 2-mm radius rounding corner is adopted as the selected configuration of the ultrasonic scalpels.

Given the vibration frequency of 120 kHz, there are two independent parameters for the structural optimization, according to Eq. (5) and Eq. (6). Thus, L_2 and L_6 are selected as the optimization variables. The optimization is conducted by traversing the optimization variables within the constraints to maximize the output vibration speed.

For this optimization, the range of L_6 is constrained from 9.0 mm to 11.0 mm, since the cutting tip length of the existing ultrasonic scalpel is usually around 10.0 mm. The L_2 should be larger than 2.0 mm for prepressing of the piezo stack. The 40-mm transducer total length limitation is adopted for ideal laparoscopic intervention. For each group of the optimization variables (L_2 and L_6), other length parameters are obtained by solving Eq. (5) and Eq. (6). Then, the finite-element modal analysis is performed to obtain the transducer's longitudinal vibration frequency, where L_4 and L_5 are tuned to ensure that the transducer's longitudinal vibration frequency is 120kHz. Then the frequency response analysis is carried out to calculate the vibration speed and stress distribution of the transducer. Please note that the vibration speed is considered an indicator of the ultrasonic scalpel's operation efficiency, which is selected as the optimization indicator. At equivalent vibration speeds, cutting efficiency remains consistent across various frequencies.

The amplitude and stress distribution are read out from the finite-element harmonic response analysis plots. The influences of the design variables on the maximum stress are insignificant. At a transducer amplitude of 9.2 μm which corresponds to the vibration speed threshold (7m/s) of tissue cutting, the maximum stress ranges from 160 MPa to 170 MPa.

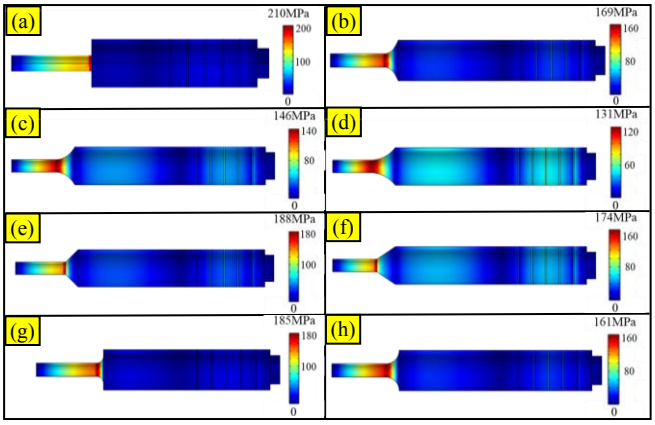

Fig. 4 The stress results corresponding to different transition structures at 9.2μm amplitude: (a) step shape; (b-d) catenary, lengths of 2mm, 3mm, and 4mm; (e-f) conical, lengths of 2mm and 3mm; (g-h) rounding corner, radius of 1mm and 2mm.

TABLE IV. DESIGN PARAMETERS AND PERFORMANCE OF THE FULL-WAVELENGTH TRANSDUCER

Transition structure	Transition structure length (mm)	Unit voltage vibration speed (m/s)	Maximum stress (MPa)	Total length of transducer (mm)
Step-shape	/	0.0702	210	32.13
Catenary	2	0.0722	169	40.53
	3	0.0665	146	41.58
	4	0.0590	131	41.98
Conical	2	0.0684	188	41.27
	3	0.0570	174	41.89
Rounding corner	Radius-1mm	0.0669	185	36.27
	Radius-2mm	0.0724	161	39.99

As shown in Fig. 5, the L_2 is traversed from 2.0 mm to 6.0 mm with a 0.5 mm interval and the L_6 is traversed from 9.0 mm to 11.0 mm with a 0.2mm interval. The output vibration speed varies monotonically with L_2 and L_6. Within the 40-mm total length constraint, at L_2 = 2.0 mm and L_6 = 10.0 mm, the transducer achieves the highest vibration speed voltage ratio of 0.0724m/s per unit voltage. This optimization result will be used for prototyping.

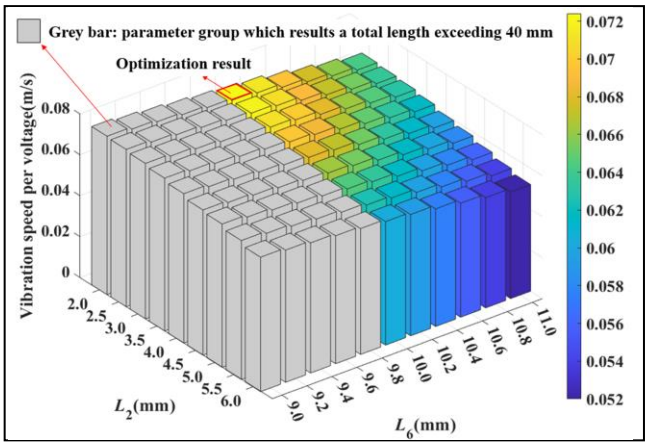

Fig. 5 The design variables and corresponding of the full-wavelength transducer: (a) the output vibration velocity per unit voltage, (b) the total length of the transducer.

Furthermore, this study investigates the influence of the cross-sectional shape of the cutting tip on the transducer's performance. The cutting tip is designed to have a flat shape, as shown in Fig.6 (a.1), and the thickness of the flat head is traversed to maximize the vibration speed. As shown in Fig. 6, in the range of 0.9-1.8mm, an increase in thickness results in a decrease in total length. Within the 40-mm total length constraint, at a thickness of 1.31 mm, the maximum vibration speed voltage ratio is 0.0771 m/s. However, the flat cutting tip design poses challenges in the machining, which is not adopted in the prototyping.

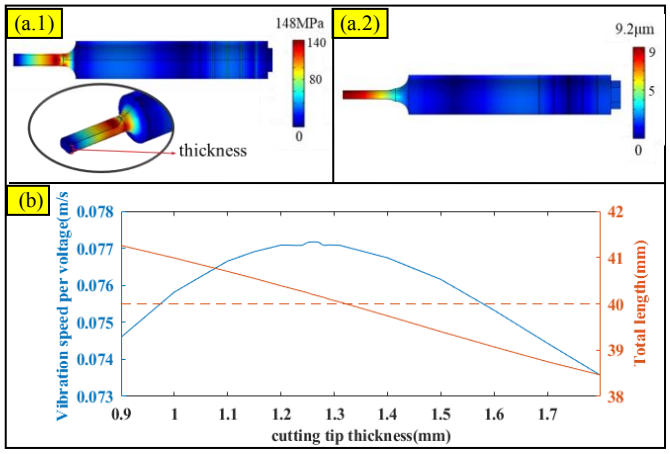

Fig. 6 (a.1-a.2) The stress and amplitude results of the harmonic simulation study for the full-wavelength ultrasonic transducer with flat-shaped amplification rod, (b) The impact on the vibration speed voltage ratio and total length with the thickness of cutting tip.

III. Experimental Validation

This section elaborates the experiments to verify the performance of the proposed full-wavelength miniature ultrasonic transducer.

As shown in Fig. 7, the components are assembled to form a prototype. The copper electrodes used in the prototype are polished to improve the contact quality. A torque wrench is used to apply pre-stress to the piezo stack.

Fig. 7 The fabricated prototype of the miniature ultrasonic transducer

A. Impedance Analysis

The impedance of the transducer was measured by an impedance analyzer (WK600B, WAYNE KERR Electronics Corp., UK). A swept signal of 1 Vrms over the bandwidth from 110 kHz to 130 kHz was applied to measure the transducer's impedance, the results are shown in Fig. 8.

The transducer's actual longitudinal vibration frequency f_r, effective electromechanical coupling factor k_{eff}, and mechanical quality factor Q_m can be derived from the impedance spectrum, where f corresponds to the minimum impedance value. k_{eff} and Q_m are calculated by Eq. (8) and (9), respectively.

$$k_{eff}^{\ 2} = \frac{f_a^2 - f_r^2}{f_a^2} \tag{8}$$

$$Q_m = \frac{f_r}{f_2 - f_1} \tag{9}$$

Where f_r and f_a are the resonance frequency and anti-resonance frequency. f_2 and f_1 correspond to the 3dB resonance impedance, with $f_2 > f_1$. For the proposed transducer, the f_r is 118.795 kHz which has a 1% error from the 120 kHz. The Q_m and k_{eff} are calculated as 642.14 and 0.2178.

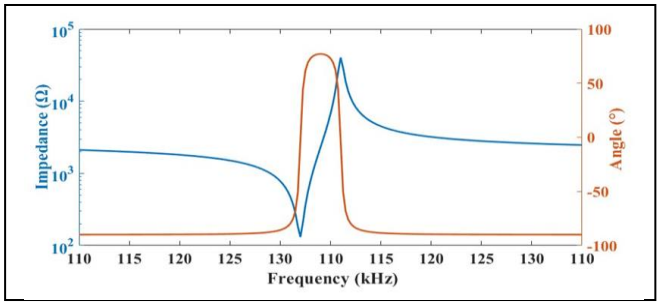

Fig. 8 The impedance curves of 120-kHz full-wavelength miniature ultrasonic transducer.

B. Vibration Speed Measurement Experiment

As shown in Fig. 9, the vibration speed of the transducer's front-end surface was measured by a single-point laser vibrometer (SOPTOP LV-S01). A 120 kHz sine excitation voltage with a peak value of 120V was generated by the signal generator, amplified by the power amplifier, and applied to the piezoelectric ceramic of the transducer for excitation.

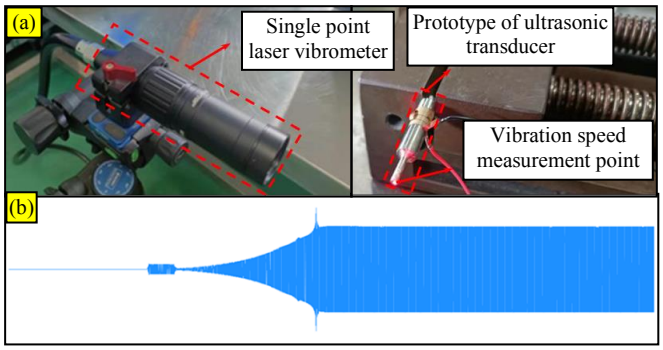

Fig. 9 The vibration speed measure experiment: (a) experiment setup, (b) the measured vibration speed curve.

The measured vibration speed curve is shown in Fig. 9(b). The peak axial amplitude speed at the transducer's tip during stable vibration measured 7.0493 m/s, exceeding the threshold for tissue cutting. This indicates the transducer prototype's feasibility for tissue-cutting applications.

C. Ex-vivo Tissue Dissection Experiment

To demonstrate the proposed transducer's tissue dissection capability, an ex-vivo tissue-cutting experiment was performed. Chicken tissue was used. During the dissection process, the transducer was mounted in a fixture.

The transducer was excited by the 120 kHz sine excitation voltage with a peak value of 120V. The chicken tissue was placed on an acrylic board and manually fed toward the transducer's cutting tip to perform dissection. The two dissection processes are shown in Fig. 10.

In cutting process 1, the chicken tissue was fed axially towards the tip of the transducer for penetration, indicating the transducer's capability for axial tissue cutting. Then the tip was moved laterally inside the tissue to perform a dissection. The total cut length and thickness were measured as 15 mm and 1mm respectively, while the process took 8.7 s.

In cutting process 2, the tissue was cut laterally by the side edge of the cutting tip, indicating the transducer's capability for lateral tissue cutting. The total cut length and thickness was measured as 12 mm and 2mm respectively, while the process took 8.3 s.

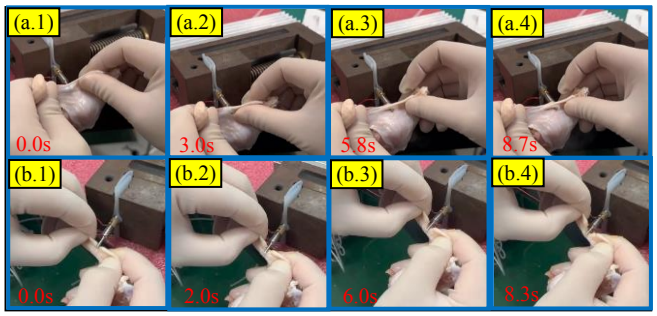

Fig. 10 Ex-vivo tissue cutting process for the full-wavelength transducer prototype: (a.1)-(a.4) cutting process 1, (b.1)-(b.4) cutting process 2.

IV. Conclusions and Future Works

This paper proposes a full-wavelength miniature Langevin ultrasonic transducer with a 6 mm diameter and indicates promising performance. The transducer can be further mounted on the 8 mm dexterous instrument, which can be potentially integrated into the surgical robotic system. The vibration model, structure design, finite-element model-based parameter optimization, prototyping, experimental verifications are elaborated in the paper.

In the design process, the vibration model is first used to calculate the structure parameters of the full-wavelength transducer with a given 120kHz vibration frequency. Then the finite-element model is used to optimize the structure parameters and maximize. The full-wavelength transducer achieves a higher vibration speed voltage ratio while meeting dimension requirements for laparoscopic intervention.

A prototype of the full-wavelength transducer is fabricated. The impedance analysis shows the actual resonance frequency of the transducer is 118.795 kHz, while its Q_m and k_{eff} are 642.14 and 0.2178. The vibration speed measurement experiment showed the transducer's peak vibration speed of over 7 m/s under the 120V excitation, while the ex-vivo tissue cutting experiment demonstrated its capability of performing tissue dissection.

Future works mainly include the integration of the transducer into a continuum instrument to construct an ultrasonic scalpel with enhanced distal dexterity and investigate its performance in the single-port surgical robotic system.

References

[1] A. Cuschieri, "Laparoscopic Surgery: Current Status, Issues and Future Developments," *The Surgeon,* vol. 3, No.3, pp. 125-138, June 2005.

[2] N. Tamini, M. Rota, E. Bolzonaro, L. Nespoli, A. Nespoli, M. G. Valsecchi, and L. Gianotti, "Single-Incision Versus Standard Multiple-Incision Laparoscopic Cholecystectomy: A Meta-analysis of Experimental and Observational Studies," *Surgical Innovation,* vol. 21, No.5, pp. 528-545, Oct 2014.

[3] S. DiMaio, M. Hanuschik, and U. Kreaden, "The da Vinci Surgical System," in *Surgical Robotics: Systems Applications and Visions*, J. Rosen, Ed., 2011, pp. 199-217.

[4] J. H. Kaouk, G.-P. Haber, R. Autorino, S. Crouzet, A. Ouzzane, V. Flamand, and A. Villers, "A Novel Robotic System for Single-port Urologic Surgery: First Clinical Investigation," *European Urology,* vol. 66, No.6, pp. 1033-1043, Dec 2014.

[5] Y. Chen, C. Zhang, Z. Wu, J. Zhao, B. Yang, J. Huang, Q. Luo, L. Wang, and K. Xu, "The SHURUI System: A Modular Continuum Surgical Robotic Platform for Multiport, Hybrid-Port, and Single-Port Procedures," *IEEE/ASME Transactions on Mechatronics,* vol. 27, No.5, pp. 3186-3197, Oct 2022.

[6] D. Kunde and C. Welch, "Ultracision in Gynaecological Laparoscopic Surgery," *Journal of Obstetrics and Gynaecology,* vol. 23, No.4, pp. 347-352, 2003.

[7] N. Družijanić, Z. Pogorelić, Z. Perko, I. Mrklić, and S. Tomić, "Comparison of Lateral Thermal Damage of the Human Peritoneum Using Monopolar Diathermy, Harmonic scalpel and LigaSure," *Canadian Journal of Surgery,* vol. 55, No.5, pp. 317-321, 2012.

[8] R. Wakako and M. Hashimoto, "Development of Ultrasonically Activated Bending Scalpel for Endoscopic Surgery," in *IEEE/RSJ International Conference on Intelligent Robots and Systems (IROS)*, EPFL, Lausanne, Switzerland, 2002, pp. 1415-1420.

[9] I. Khalaji, M. D. Naish, and R. V. Patel, "Articulating Minimally Invasive Ultrasonic Tool for Robotics-Assisted Surgery," in *IEEE International Conference on Robotics and Automation (ICRA)*, Seattle, Washington, 2015, pp. 573-578.

[10] J. Li, H. Liu, J. Li, Y. Yang, and S. Wang, "Piezoelectric Transducer Design for an Ultrasonic Scalpel with Enhanced Dexterity for Minimally Invasive Surgical Robots," *Proceedings of the Institution of Mechanical Engineers, Part C: Journal of Mechanical Engineering Science,* vol. 234, No.7, pp. 1271-1285, Dec 2020.

[11] X. Li, T. Stritch, K. Manley, and M. Lucas, "Limits and Opportunities for Miniaturizing Ultrasonic Surgical Devices Based on a Langevin Transducer," *IEEE Transactions on Ultrasonics, Ferroelectrics, and Frequency Control,* vol. 68, No.7, pp. 2543-2553, March 2021.

[12] D. A. DeAngelis, "Predicting the Displacement Gain from the Mechanical Quality Factor in Ultrasonic Transducers," *Physics Procedia,* vol. 87, pp. 2-9, 2016.